

Electrochemical and spectroelectrochemical studies on platinum complexes containing 2,2'-bipyridine†

David Collison,^a Frank E. Mabbs,^a Eric J. L. McInnes,^{*b} Kenneth J. Taylor,^a Alan J. Welch^b and Lesley J. Yellowlees^{*b}

^a Department of Chemistry, University of Manchester, Manchester M13 9PL, UK

^b Department of Chemistry, University of Edinburgh, Edinburgh EH9 3JJ, UK

The electrochemical and spectroelectrochemical (UV/VIS/NIR and EPR) properties of a series of complexes of general formula $[\text{Pt}(\text{bipy})\text{L}_2]^{n+}$ ($\text{L} = \text{Cl}^-$ or CN^- , $n = 0$; $\text{L} = \text{NH}_3$, py, PMe_3 or $\text{L}_2 = \text{en}$, $n = 2$; bipy = 2,2'-bipyridine, py = pyridine, en = ethylenediamine) have been investigated. The complexes undergo a reversible one-electron reduction process at potentials of ca. -1 V vs. Ag–AgCl. In each case UV/VIS/NIR spectra of the one-electron reduction products were consistent with co-ordinated bipyridyl anion-radical species rather than d^9 metal centres. Electron paramagnetic resonance spectra of the chemically or electrochemically generated 17-electron species, in conjunction with the results of extended-Hückel molecular-orbital calculations, show a significant admixture of metal $5d_{yz}$ and/or $6p_z$ orbitals in the singly-occupied molecular orbital. The complex $[\text{Pt}(\text{bipy})(\text{PMe}_3)_2][\text{BF}_4]_2$ has been prepared.

Few monomeric formally platinum(II) complexes are known. Most reported examples are generated by the one-electron reduction of platinum(II) species. α -Diimine complexes in particular have been the subject of much research with respect to forming d^9 metal centres.^{1–6} In this work we have studied the reduction products of a series of complexes of general formula $[\text{Pt}(\text{bipy})\text{L}_2]^{n+}$ [$\text{L} = \text{Cl}^-$ or CN^- , $n = 0$; $\text{L} = \text{NH}_3$, pyridine (py), PMe_3 or $\text{L}_2 = \text{ethylenediamine}$ (en), $n = 2$; bipy = 2,2'-bipyridine] and have electronically characterised the redox-active orbital *via* spectroelectrochemical techniques (UV/VIS/NIR and EPR) in conjunction with extended-Hückel molecular-orbital (EHMO) calculations.

Miskowski and Holding⁷ assigned the lowest unoccupied molecular orbital (LUMO) of $[\text{Pt}(\text{bipy})\text{Cl}_2]$ and $[\text{Pt}(\text{bipy})(\text{en})]^{2+}$ as metal and ligand based, respectively, on the basis of their absorption and emission spectra. Electrochemical studies show that such species typically undergo two consecutive one-electron reductions.^{1,2,8} Braterman *et al.*^{1,2} concluded from *in situ* UV/VIS/NIR and EPR spectroelectrochemical experiments on $[\text{Pt}(\text{bipy})(\text{en})]^{2+}$, $[\text{Pt}(\text{bipy})(\text{py})_2]^{2+}$ and $[\text{Pt}(\text{bipy})\text{Ph}_2]$ that the first reduction process is ligand based whilst the second reduction process is metal based. We report here a more detailed analysis of the spectroscopy of the reduced 17-electron species.

Experimental

The complexes $[\text{Pt}(\text{bipy})\text{Cl}_2]$ **1**,⁹ $[\text{Pt}(\text{bipy})(\text{NH}_3)_2]^{2+}$ **2**,¹⁰ $[\text{Pt}(\text{bipy})(\text{en})]^{2+}$ **3**,¹¹ $[\text{Pt}(\text{bipy})(\text{py})_2]^{2+}$ **4**¹¹ and $[\text{Pt}(\text{bipy})(\text{CN})_2]$ **6**¹¹ were prepared by literature methods. The complex $[\text{Pt}(\text{bipy})(\text{PMe}_3)_2]^{2+}$ **5** was prepared as follows. Trimethylphosphine in tetrahydrofuran (2.2 cm^3 of 1.0 mol dm^{-3} solution, $2.2 \times 10^{-3} \text{ mol PMe}_3$) was syringed into an $\text{N}_2(\text{g})$ saturated suspension of $[\text{Pt}(\text{bipy})\text{Cl}_2]$ (0.455 g , $1.08 \times 10^{-3} \text{ mol}$) in water (50 cm^3) and heated under reflux in an atmosphere of $\text{N}_2(\text{g})$ with stirring until the suspension had dissolved to give a yellow solution. Addition of NaBF_4 (0.5 g , excess) yielded an immediate yellow precipitate which was collected, washed with water and air dried. Recrystallisation twice from water gave yellow needles of the desired product (0.45 g , 62%) (Found: C, 28.4; H, 3.2; N, 5.2%. Calc. for

$\text{C}_{16}\text{H}_{26}\text{B}_2\text{F}_8\text{N}_2\text{P}_2\text{Pt}$: C, 28.4; H, 3.9; N, 4.1%). $^{31}\text{P}\{-^1\text{H}\}$ NMR (200 MHz, CD_3NO_2): $\delta -27.46$ (s, ^{195}Pt satellites, $J_{\text{Pt}} = 3423 \text{ Hz}$). The $^{31}\text{P}\{-^1\text{H}\}$ NMR spectrum was recorded on a Bruker WP200SY spectrometer and was externally referenced to 85% aqueous H_3PO_4 .

Electrochemical studies were performed using a DSL 286-D PC with General Purpose Electrochemical System (GPES) Version 3 software connected to an Autolab system containing a PSTAT10 potentiostat. Cyclic voltammetry used a standard three-electrode configuration with platinum microworking and counter electrodes and an Ag–AgCl reference electrode against which the ferrocene–ferrocenium couple was measured at $+0.55$ V. Redox potentials and peak-to-peak values are reported for a scan rate of 100 mV s^{-1} . Bulk electrolysis was performed in a compartmentalised H-cell with platinum grid working and counter electrodes, the reference electrode was as before. All electrochemical studies were performed on nitrogen purged *N,N'*-dimethylformamide (dmf) solutions at 243 K containing $0.1 \text{ mol dm}^{-3} \text{ NBu}_4\text{BF}_4$.

In situ UV/VIS/NIR electrogenerations employed an optically transparent electrode (OTE) cell in a Perkin-Elmer Lambda 9 spectrophotometer.¹² Reductions were performed at 243 K as a function of potential with spectra recorded every 15 min. After each experiment was completed the electrogeneration potential was set at 0 V to regenerate the starting material in order to ensure the chemical integrity of the system. X-Band EPR data are quoted for dmf solutions at either room temperature (fluid solution in flat cell) or 77 K (frozen glass) recorded on an X-band Bruker ER200D-SCR spectrometer. Q-Band spectra at 150 K were recorded on a Varian E112 spectrometer.

The EHMO calculations used a locally modified version of ICON8^{13a} and the weighted H_{ij} formula,^{13b} and were performed on models of **1**, **2** and **6** based on published crystallographic data.^{14–16} The same Pt(bipy) fragment was used in each case with C–C and C–N bond lengths of 1.37 \AA , Pt–N 1.99 \AA and a N–Pt–N bite angle of 80° . The molecule lies in the *xy* plane with the *y* axis bisecting the N–Pt–N angle (Fig. 1). The H_{ii} s for Pt orbitals were initially optimised by charge iteration calculations [$H_{ii} = -\text{VSIE}(Q)$, where $\text{VSIE}(Q) = \text{valence state ionisation energy of orbital } i \text{ when atom has charge } Q$]. The full list of orbital exponents and H_{ii} s (eV) used is H_{1s} : $H_{ii} = -13.60$, $\zeta = 1.30$; C_{2s} : $H_{ii} = -21.40$, $\zeta = 1.625$; C_{2p} : $H_{ii} = -11.40$, $\zeta = 1.625$; N_{2s} : $H_{ii} = -26.00$, $\zeta = 1.95$;

† Non-SI unit employed: $G = (g_{\text{exp}}/2.142 \times 10^4) \text{ cm}^{-1} = 10^{-4} \text{ T}$.

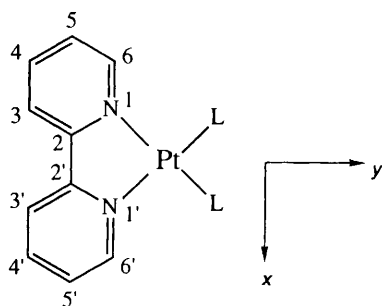


Fig. 1 Structure and numbering scheme for the complexes $[\text{Pt}(\text{bipy})\text{L}_2]^{n+}$

N_{2p} : $H_{ii} = -13.40$, $\zeta = 1.95$; Cl_{3s} : $H_{ii} = -30.00$, $\zeta = 2.033$; Cl_{3p} : $H_{ii} = -15.00$, $\zeta = 2.033$; Pt_{6s} : $H_{ii} = -10.93$, $\zeta = 2.554$; Pt_{6p} : $H_{ii} = -5.439$, $\zeta = 2.554$; Pt_{5d} : $H_{ii} = -13.52$, $\zeta_1 = 6.013$, $\zeta_2 = 2.696$, $c^1 = 0.633\ 38$, $c^2 = 0.551\ 28$, where c^1 and c^2 are the coefficients in the double- ζ expansion.

Results and Discussion

EHMO calculations

The LUMO of complex **1** is computed to be of b_2 symmetry with 96% $\text{bipy}-\pi^*$ character and small Pt $5d_{yz}$ and $6p_z$ admixtures of 2.0 and 1.7%, respectively. This corresponds to the lowest unoccupied π^* orbital of the bipy ligand, $\pi(7)$. These results agree with those of Eisenberg and co-workers¹⁷ on similar platinum bipyridyls such as $[\text{Pt}(\text{bipy})(\text{mnt})]$ ($\text{H}_2\text{mnt} = 2,3\text{-disulfanylmaleonitrile}$). The major contributions to the bipy π^* -based LUMO are from the two nitrogen nuclei and the C2, C2', C4 and C4' nuclei. We realise that the geometry of the reduced form of the complex will be different from that of the ground state but, in the absence of crystallographic data on the one-electron reduction product, the calculations will provide an upper limit to the metal participation in the singly-occupied molecular orbital (SOMO) of the reduced species.

Calculations performed for complexes **2** and **6** give similar molecular orbital schemes to that of **1**. Molecular orbital coefficients of the LUMOs are given in Table 1. The results show that the $5d_{yz}$ admixture to the primarily ligand-based orbital decreases as L changes from Cl^- (a π donor) through NH_3 (no π bonding capabilities) to CN^- (a π acceptor). Interestingly the calculations show that the $6p_z$ contribution to the LUMO increases along this series. In no case were there significant contributions from orbitals based on the L ligands.

Electrochemistry

Cyclic voltammetric studies of complexes **1–6** in $0.1\ \text{mol dm}^{-3}$ $\text{NBu}_4\text{BF}_4\text{-dmf}$ reveal a fully reversible reduction at *ca.* $-1\ \text{V}$ vs. Ag-AgCl (Table 2). There are no oxidation processes observed prior to the solvent breakdown at $+2\ \text{V}$ for any of the compounds studied. Coulometric experiments at 243 K confirm a one-electron reduction. The bulk reduction in each case is accompanied by a characteristic yellow to olive green colour change. Complexes **1–4** and **6** undergo a second reversible or quasi-reversible reduction at more negative potentials (Table 2). The separation between reductions of 500–700 mV is typical of successive reductions of co-ordinated bipyridyls although we have no spectroscopic evidence to confirm the nature of this second reduction process. The second reduction of complex **5** is irreversible, showing no anodic peak. The small variation of E_1 with L is highly indicative of a similar electronic character of the redox-active orbital in each case.

UV/VIS/NIR spectroelectrochemistry

The electronic spectra of complexes **1–6** in dmf are dominated by the intense intraligand $\pi \rightarrow \pi^*$ bands of the bipy ligand and

Table 1 Molecular orbital coefficients for the LUMO of complexes **1**, **2** and **6**

Atom	Orbital	1	2	6
N1, N1'	$2p_z$	0.129	0.128	0.107
C2, C2'	$2p_z$	0.130	0.131	0.120
C3, C3'	$2p_z$	0.003	0.003	0.032
C4, C4'	$2p_z$	0.117	0.118	0.109
C5, C5'	$2p_z$	0.046	0.046	0.040
C6, C6'	$2p_z$	0.055	0.055	0.055
Pt	$5d_{yz}$	0.020	0.020	0.012
	$6p_z$	0.017	0.018	0.042
C7, C7'	$2p_z$	—	—	0.024
N2, N2'	$2p_z$	—	—	0.015

* Complex **6** only, L = CN^- where C = C7, C7'; N = N2, N2'.

Table 2 Redox potentials of $[\text{Pt}(\text{bipy})\text{L}_2]^{n+}$ in $0.1\ \text{mol dm}^{-3}$ $\text{NBu}_4\text{BF}_4\text{-dmf}$ at 293 K

Complex	E_1/V	E_2/V
1	-1.06^a (0.070) ^b	-1.79 (0.110)
2	-0.99 (0.060)	-1.65 (0.080)
3	-0.90 (0.070)	-1.56 (0.070)
4	-0.91 (0.060)	-1.45 (0.070)
5	-0.94 (0.060)	-1.48^c
6	-0.94 (0.060)	-1.61 (0.090)

^a $(E_f + E_r)/2$. ^b $(E_f - E_r)$. ^c Anodic peak not observed, cathodic peak quoted.

Table 3 UV/VIS data for $[\text{Pt}(\text{bipy})\text{L}_2]^{n+}$ in dmf solution *

Complex	$10^{-3}\ \text{m.l.c.t./cm}^{-1}$	$10^{-3}\ \pi \rightarrow \pi^*/\text{cm}^{-1}$
1	25.7 (0.45)	30.8 (1.28), 32.0 (1.19)
2	29.4 (0.33) (sh)	31.1 (1.67), 32.3 (1.35)
3	29.4 (0.41) (sh)	31.2 (2.25), 32.4 (1.86)
4	29.8 (0.41) (sh)	31.1 (1.70), 32.4 (1.43)
5	27.4 (0.12) (sh)	30.9 (1.24), 31.8 (1.05)
6	29.4 (sh)	31.3, 32.6 (sh)

* Values of $10^{-4}\ \epsilon$ ($\text{dm}^3\ \text{mol}^{-1}\ \text{cm}^{-1}$) are in parentheses.

a lower energy metal-to-ligand [bipy $\pi(7)$] charge transfer (m.l.c.t.) band, which appears as a shoulder for complexes **2–6** but is clearly resolved for **1**. These assignments (Table 3) are in agreement with those of Gidney *et al.*¹⁸

The spectral changes of complex **1** on reduction to $\mathbf{1}^-$ in $0.1\ \text{mol dm}^{-3}$ $\text{NBu}_4\text{BF}_4\text{-dmf}$ at 243 K (Fig. 2) are consistent with the redox orbital being the lowest unoccupied antibonding π^* orbital of the bipy ligand.^{19,20} The bands at 11 200, 20 100, 21 600 and 27 900 cm^{-1} can all be assigned as intraligand transitions of co-ordinated bipy⁻ by direct comparison with the UV/VIS/NIR spectrum of Na^+bipy^- .²⁰ The band at 23 900 cm^{-1} cannot be assigned to an internal bipy⁻ transition as there is no analogous band in the spectrum of Na^+bipy^- . We therefore assign this as a charge transfer (c.t.) transition.

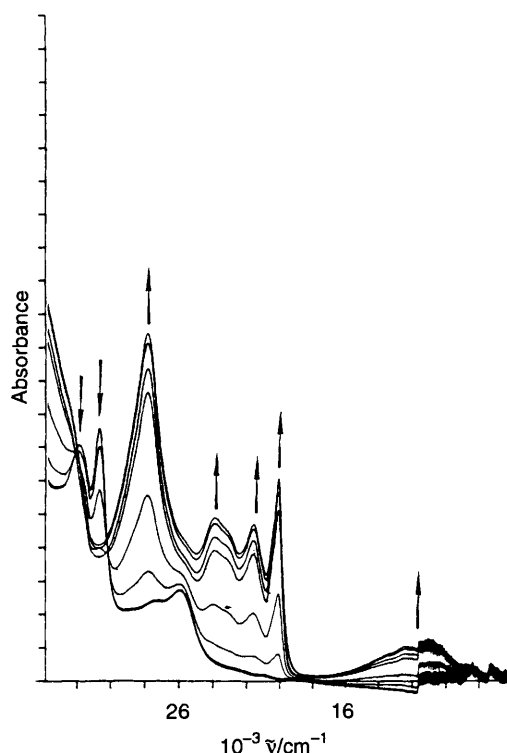
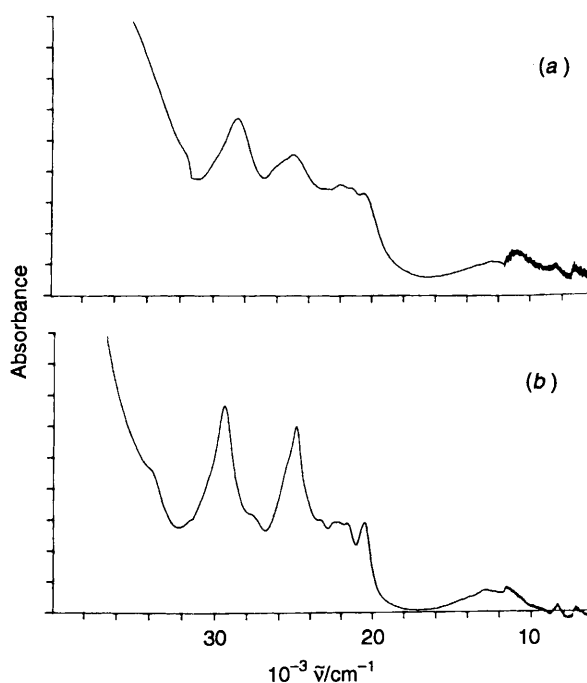
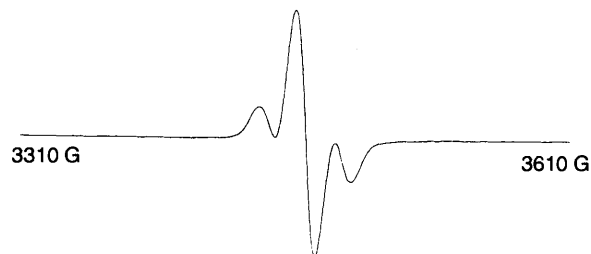
Complexes **2–6** exhibit similar spectra to each other and to $\mathbf{1}^-$ on reduction and may be assigned as above. Typical spectra of the reduced complexes are shown in Fig. 3 and the proposed assignments of the electronic transitions are given in Table 4. The reduced species were found to be unstable at ambient temperatures, as witnessed by the absorption spectrum failing to return to that of the parent species on reoxidation of the solution.

Thus we conclude from consideration of the UV/VIS/NIR spectroelectrochemical experiments that the one-electron reduction products should be formulated as $[\text{Pt}^{\text{II}}(\text{bipy}^-)\text{L}_2]^{(n-1)+}$. The second reduction product of $[\text{Pt}(\text{bipy})\text{L}_2]^{n+}$ in each case proved too unstable at any temperature studied (293–243 K) for definitive investigations.

Table 4 UV/VIS/NIR data for $[\text{Pt}(\text{bipy})\text{L}_2]^{(n-1)+}$ in $0.1 \text{ mol dm}^{-3} \text{NBu}_4\text{BF}_4\text{-dmf}$ at 243 K^a

Complex	$10^{-3} \pi(7-8,9)^*/\text{cm}^{-1}$	$10^{-3} \pi(7-10)^*/\text{cm}^{-1}$	$10^{-3} \text{c.t.}/\text{cm}^{-1}$	$10^{-3} \pi(6-7)^*/\text{cm}^{-1}$
Na(bipy) ^c	12.0 (0.15)	17.8 (0.62), 18.8 (0.62)	—	25.9 (2.95)
1 ⁻	11.2 (0.21)	20.1 (1.00), 21.6 (0.54)	23.9 (0.81)	27.9 (1.72)
2 ⁻	12.4 (0.23)	19.7 (0.54), 20.9 (0.57)	24.8 (0.53)	28.0 (1.10)
3 ⁻	12.4 (0.33)	20.5 (0.68), 22.0 (0.65)	24.8 (1.14)	29.3 (1.35)
4 ⁻	10.7 (0.24)	20.4 (0.51), 22.0 (0.57)	24.9 (0.73)	28.4 (0.92)
5 ⁻	11.4 (0.13)	20.6 (0.44), 22.1 (0.41)	24.7 (0.63)	28.9 (0.65)
6 ⁻	11.5	20.5, 22.0	24.9	29.4

^a Values of $10^{-4} \epsilon (\text{dm}^3 \text{mol}^{-1} \text{cm}^{-1})$ are in parentheses. ^b Transitions assigned by comparison with Na(bipy). ^c thf Solution, ref. 20.

**Fig. 2** Optically transparent electrode reduction of complex 1 to 1⁻ in $0.1 \text{ mol dm}^{-3} \text{NBu}_4\text{BF}_4\text{-dmf}$ at 243 K**Fig. 3** UV/VIS/NIR spectra of 4⁻ (a) and 6⁻ (b) in $0.1 \text{ mol dm}^{-3} \text{NBu}_4\text{BF}_4\text{-dmf}$ at 243 K**Fig. 4** Solution EPR spectrum of 3⁻ in dmf at 293 K

EPR spectroelectrochemistry

The solution spectra of the one-electron reduction products of complexes 1–6 in dmf at room temperature are as expected for interaction of the unpaired electron with platinum in natural abundance (¹⁹⁵Pt, 34%, spin 1/2). A typical spectrum for complexes 1⁻–5⁻ is shown in Fig. 4. The isotropic hyperfine coupling constants for 1⁻–5⁻ are in the range $(40\text{--}55) \times 10^{-4} \text{ cm}^{-1}$ (Table 5). The reduction products can be generated electrochemically or chemically (with an excess of NaBH₄) to give rise to identical spectra, *i.e.* the reduction product is the same regardless of the method of generating the sample.

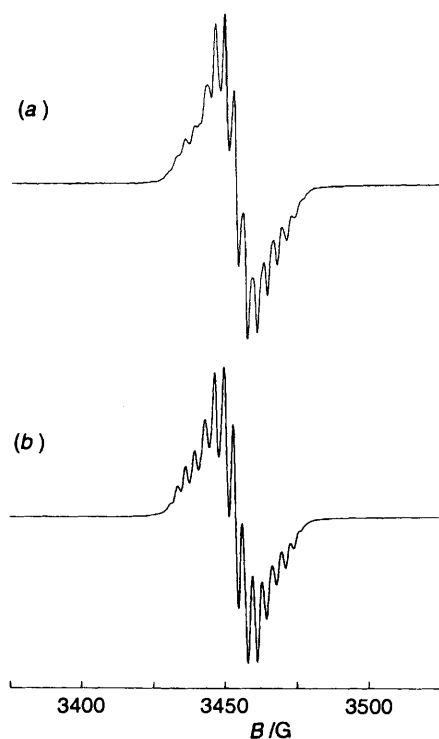
The isotropic EPR signals of ions 1⁻–5⁻ show that the coupling of the unpaired electron is observed solely to the Pt nucleus, with any coupling to ligand nuclei unresolved and therefore much smaller in magnitude. This is not to say that we wish to interpret the spectra in terms of a d⁹ system (see below). Direct admixture of the Pt 6s orbital to the SOMO of b₂ symmetry is forbidden in C_{2v} point symmetry and consequently the isotropic hyperfine coupling must arise *via* inner-core polarisation. The contribution to the isotropic hyperfine interaction from inner-core polarisation is given by $-\kappa P$,²¹ where κ is an empirical parameter which is positive for d transition-metal ions²² and P is given by the expression $P = 2.0023g_n\beta_N\beta_e\langle r^{-3} \rangle$ (where g_n is the nuclear gyromagnetic ratio, β_N and β_e are the nuclear and electron magnetons respectively and r is the spatial coordinate) and has been evaluated at $+492 \times 10^{-4} \text{ cm}^{-1}$ for ¹⁹⁵Pt,²³ and hence we assign our A_{iso} as negative in sign.

For ion 6⁻, superhyperfine coupling of the unpaired electron to nuclei of the bipy ligand is observed, see Fig. 5(a), indicating extensive delocalisation of the odd electron onto the ligand set giving rise to a bipyridyl anion radical species. Variable temperature (293–223 K) studies on 6⁻ show superimposable signals. A good simulation of this spectrum was obtained, see Fig. 5(b), assuming coupling to ¹⁹⁵Pt ($A_{\text{iso}} = 20.5 \text{ G}$, $19.1 \times 10^{-4} \text{ cm}^{-1}$), to two equivalent ¹⁴N nuclei [$a_{\text{iso}}(^{14}\text{N}) = 3.4 \text{ G}$], to two sets of two equivalent ¹H nuclei [$a_{\text{iso}}(1) = 2.8$ and $a_{\text{iso}}(2) = 2.2 \text{ G}$] and a Lorentzian linewidth of 1.7 G.²⁴ We assign the larger ¹H coupling to H⁴ and H^{4'}, and the ¹⁴N coupling to the ring nitrogen atoms of the bipy ligand in agreement with the EHMO calculations. The smaller ¹H coupling has not been assigned as the calculations do not favour another pair of ¹H nuclei. Splitting to the other ¹H nuclei is unresolved and therefore smaller than the observed linewidth.

Table 5 EPR parameters for $[\text{Pt}(\text{bipy})\text{L}_2]^{(n-1)+}$

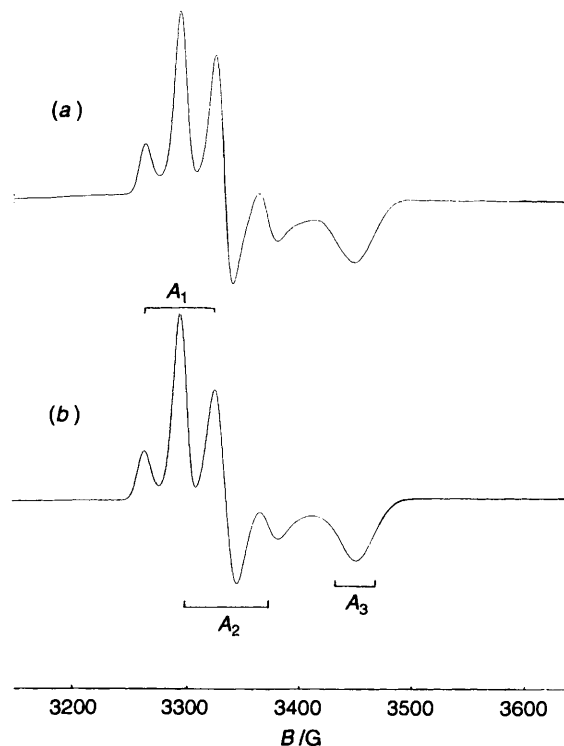
		g_{iso}^a	g_1^b	g_2	g_3	$A_{\text{iso}}(\text{Pt})^c$	A_1	A_2	A_3
1^-	<i>d</i>	1.998	2.038	2.009	1.935	-54	-56	-95	—
	<i>e</i>	—	2.038	2.011	1.938	—	-57.4	-80.6	-20.8
2^-	<i>d</i>	1.998	2.029	2.003	1.936	-40	-59	-91	—
	<i>e</i>	—	2.027	2.002	1.936	—	-58.2	-71.2	-31.6
3^-	<i>d</i>	1.998	2.026	2.009	1.954	-42	-53	-78	—
4^-	<i>d</i>	1.994	2.017	2.004	1.960	-40	-60	-75	—
	<i>e</i>	—	2.018	2.004	1.960	—	-56.5	-65.5	-27.5
5^-	<i>d</i>	1.999	2.022	2.016	1.970	—	-56	-65	—
6^-	<i>d, f</i>	1.994	2.013	2.009	1.974	—	-38	-49	—
	<i>e, f</i>	1.994 ^g	2.014	2.009	1.974	-19.1 ^g	-35.7	-38.5	+27.6

^a Isotropic data from chemically generated species, dmf solution. ^b Anisotropic data from electrochemically generated species, 0.1 mol dm⁻³ NBu₄BF₄-dmf. ^c 10^4 A/cm⁻¹. ^d Parameters estimated from the spectra. ^e Parameters from computer simulations. ^f Q-Band spectrum. ^g From simulations as described in the text.

**Fig. 5** Solution EPR spectrum of 6^- in dmf at 293 K (a) and simulation using the parameters given in the text (b)

The EHMO calculations show that the nitrogen atoms of the cyanide ligands should make little contribution to the SOMO. Rieger and co-workers²⁵ assigned the largest ¹H couplings in the isotropic EPR spectra of species such as *mer*-[Mn(CO)(CNBu^t)₃(bipy⁻)] similarly. The isotropic coupling to ¹⁹⁵Pt is considerably smaller in 6^- (19.1×10^{-4} cm⁻¹) than for 1^- – 5^- [$(40\text{--}55) \times 10^{-4}$ cm⁻¹], hence we suggest that it is this that allows the resolution of the superhyperfine structure in the EPR spectrum of $[\text{Pt}(\text{bipy})(\text{CN})_2]^-$.

On freezing the solutions at 77 K, the X-band EPR spectra exhibit rhombic *g* and *A* matrices, see Figs. 6–9 and Table 5.¹² The high-field component of each of these spectra (g_3) does not show any resolution of the ¹⁹⁵Pt coupling and the values of A_3 in Table 5 are those required to give the best fit between experimental and simulated spectra. Experiments with mixed solvent systems also failed to give resolution of this g_3 component. Excellent simulations of the X-band spectra of 1^- ,¹² 2^- and 4^- were obtained using the parameters in Table 5.²⁶ The magnitudes of A_3 have a probable uncertainty of *ca.* $\pm 5 \times 10^{-4}$ cm⁻¹ due to the lack of resolution of the g_3 components of these spectra. Fig. 6 shows typical experimental and simulated spectra. For 1^- – 4^- the averaged values of *g* and

**Fig. 6** X-Band EPR spectrum of 2^- in 0.1 mol dm⁻³ NBu₄BF₄-dmf at 77 K (a) and simulation using the parameters in Table 5 with Gaussian linewidths of 11, 16 and 23 G for g_1 , g_2 and g_3 , respectively (b)

A used in the simulations are in good agreement with the experimental isotropic values and hence A_1 , A_2 and A_3 all have the same sign as each other and A_{iso} . The frozen solution spectra of 5^- and 6^- appear to be axial at X-band frequency [Figs. 8 and 9(a)] but the rhombicity in 6^- is clearly shown in its Q-band spectrum at 150 K, see Fig. 9(b). Since the X-band spectra of 6^- show no changes between 150 and 77 K we assume that the same anisotropy is present at 77 K as at 150 K. For 6^- a good simulation of the Q-band spectrum was obtained, see Fig. 9(c), with the parameters in Table 5. In order that the averaged values of A_1 , A_2 and A_3 are compatible with A_{iso} , it is necessary to have A_3 opposite in sign to A_1 , A_2 and A_{iso} . The physical ramifications of this change in sign of A_3 are, as yet, unclear. No superhyperfine splittings have been resolved in any of the frozen-solution spectra. The small shift in g_{iso} from the free-electron value of 2.0023 is suggestive of only a small admixture of metal orbitals in the SOMO, and that on reduction the electron is therefore localised mainly on the bipy ligand. However, in the frozen-solution spectrum, one *g* value, g_3 , is always significantly less than 2.0023. This is indicative of the presence of at least one excited state arising from the excitation

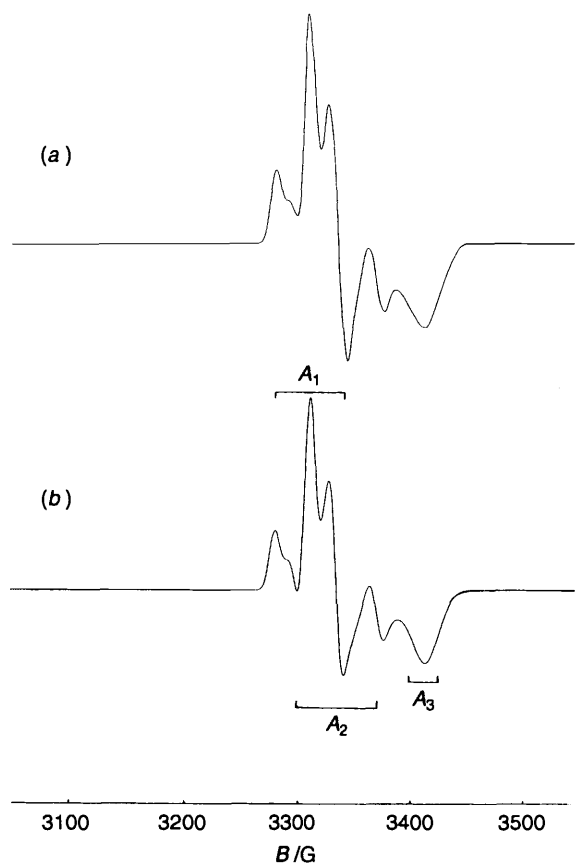


Fig. 7 X-Band EPR spectrum of 4^- in $0.1 \text{ mol dm}^{-3} \text{NBu}_4\text{BF}_4\text{-dmf}$ at 77 K (a) and simulation using the parameters in Table 5 with Gaussian linewidths of 9, 10 and 18 G for g_1 , g_2 and g_3 , respectively (b)

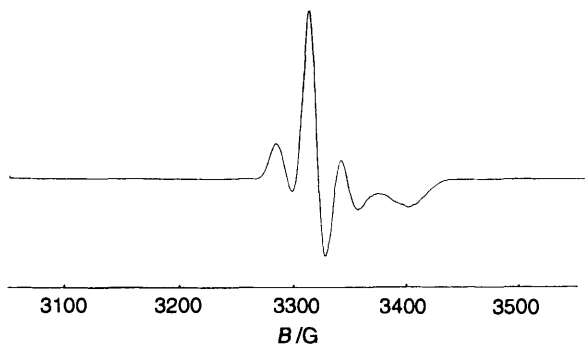


Fig. 8 X-Band EPR spectrum of 5^- in $0.1 \text{ mol dm}^{-3} \text{NBu}_4\text{BF}_4\text{-dmf}$ at 77 K

of the single electron from the SOMO to an unfilled molecular orbital (UMO). The value of g_3 and the mechanism whereby the deviation of g_3 from 2.0023 occurs indicates significant metal-orbital participation in both the SOMO and UMO.²⁷ The results of our EHMO calculations on the Pt^{II} compounds indicate that the only Pt orbitals of the correct symmetry and energy to mix with the predominantly π^* ligand-based LUMO of b_2 symmetry are the $5d_{yz}$ and $6p_z$. Using established procedures^{*28,29} for analysing the ^{195}Pt hyperfine data, we can estimate the Pt 5d contribution to the SOMO of $[\text{Pt}(\text{bipy})\text{L}_2]^{(n-1)+}$ at ca. 10%. This is similar to the value given by the EHMO calculations of the Pt^{II} analogues. However, this treatment neglects any $6p_z$ contributions which our EHMO calculations on **1**, **2** and **6** suggest may be of equal importance to the $5d_{yz}$. We are now attempting to solve the non-trivial EPR equations which contain contributions from both 6p and

* We used the calculated value of the anisotropic hyperfine parameter for ^{195}Pt for unit population of $+492 \times 10^{-4} \text{ cm}^{-1}$.²³

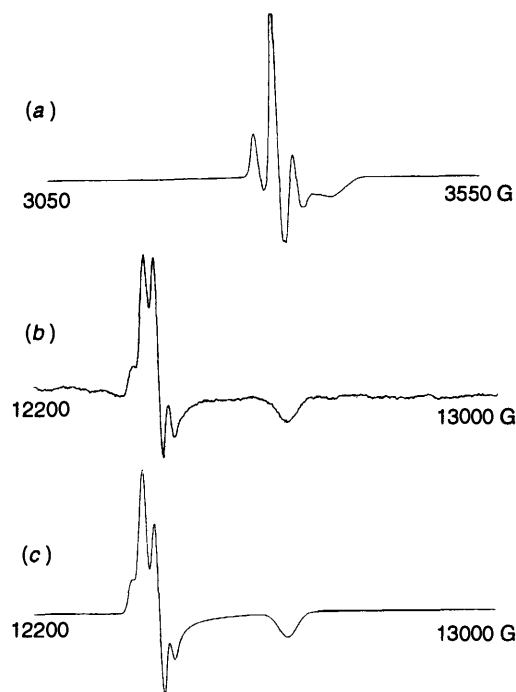


Fig. 9 X-Band EPR spectrum of 6^- in $0.1 \text{ mol dm}^{-3} \text{NBu}_4\text{BF}_4\text{-dmf}$ at 77 K (a), Q-band EPR spectrum of **6** in dmf at 150 K (b) and simulation using the parameters in Table 5 with Gaussian linewidths of 12, 11 and 26 G for g_1 , g_2 and g_3 , respectively (c)

5d orbitals which will then allow us to reinterpret the EPR data in more detail.

The inherently large hyperfine splittings for the ^{195}Pt nucleus^{23,30} compared to the ligand nuclei (^{14}N , ^1H) result in much larger observed hyperfine coupling constants for ^{195}Pt for similar contributions to the SOMO. Thus, although the SOMO of $[\text{Pt}(\text{bipy})\text{L}_2]^{(n-1)+}$ is predominantly bipy based, with small (ca. 10%) admixtures of Pt orbitals, their EPR spectra are dominated by the metal splittings.

Conclusion

The UV/VIS/NIR spectroelectrochemical results show the first one-electron reduction of $[\text{Pt}(\text{bipy})\text{L}_2]^{n+}$ to be a ligand-localised process yielding $[\text{Pt}^{\text{II}}(\text{bipy}^-)\text{L}_2]^{(n-1)+}$. However, EPR results indicate a significant amount of metal orbital mixing with the mainly bipy-based orbital. The electrochemical results are in good agreement with the electronic assignment of the LUMO of all the complexes $[\text{Pt}(\text{bipy})\text{L}_2]^{n+}$ as bipy-Pt delocalised.

Acknowledgements

We thank the Wolfson (Scotland) Trust (E. J. L. M.), the Royal Society of London (D. C.) and the EPSRC for funding.

References

- 1 P. S. Braterman, J.-I. Song, C. Vogler and W. Kaim, *Inorg. Chem.*, 1992, **31**, 222.
- 2 P. S. Braterman, J.-I. Song, F. M. Wimmer, S. Wimmer, W. Kaim, A. Klein and R. D. Peacock, *Inorg. Chem.*, 1992, **31**, 5084.
- 3 R. J. Klinger, R. J. Huffman and J. K. Kochi, *J. Am. Chem. Soc.*, 1982, **104**, 2147.
- 4 W. A. Fordyce, K. H. Pool and G. A. Crosby, *Inorg. Chem.*, 1982, **21**, 1027.
- 5 A. Jouaiti, M. Geoffroy, G. Terron and G. Bernardinelli, *J. Am. Chem. Soc.*, 1995, **117**, 2251.
- 6 S. Hasenzahl, H.-D. Hausen and W. Kaim, *Chem. Eur. J.*, 1995, **1**, 95.
- 7 V. M. Miskowski and V. H. Holding, *Inorg. Chem.*, 1989, **28**, 1529.

- 8 J. A. Zuleta, M. S. Burbery and R. Eisenberg, *Coord. Chem. Rev.*, 1990, **97**, 47.
- 9 G. T. Morgan and F. H. Burstall, *J. Chem. Soc.*, 1934, 965.
- 10 H. M. Colquhoun, J. F. Stoddart, D. J. Williams, J. B. Wolstenholme and R. Zarzycki, *Angew. Chem., Int. Ed. Engl.*, 1981, **20**, 1051.
- 11 E. Bielli, P. M. Gidney, R. D. Gillard and B. T. Heaton, *J. Chem. Soc., Dalton Trans.*, 1974, 2133.
- 12 S. A. Macgregor, E. J. L. McInnes, R. J. Sorbie and L. J. Yellowlees, *Molecular Electrochemistry of Inorganic, Bioinorganic and Organometallic Compounds*, eds. A. J. L. Pombeiro and J. A. McCleverty, Kluwer Academic Publishers, Netherlands, 1993, p. 503.
- 13 (a) J. Howell, A. Rossi, D. Wallace, K. Haraki and R. Hoffman, ICON8, QCPE, University of Indiana, 1977, no. 353; (b) J. H. Ammeter, H.-B. Burgi, J. C. Thilbeault and R. Hoffman, *J. Am. Chem. Soc.*, 1982, **100**, 3686.
- 14 R. S. Osborn and D. Rogers, *J. Chem. Soc., Dalton Trans.*, 1974, 1002.
- 15 R. H. Herber, M. Croft, B. Bilash and A. Sahiner, *Inorg. Chem.*, 1994, **33**, 2422.
- 16 C.-M. Che, L.-Y. He, C.-K. Poon and T. C. W. Mak, *Inorg. Chem.*, 1989, **28**, 3081.
- 17 J. A. Zuleta, J. M. Bevilacqua, D. M. Prosperpio, P. D. Harvey and R. Eisenberg, *Inorg. Chem.*, 1992, **31**, 2396.
- 18 P. M. Gidney, R. D. Gillard and B. T. Heaton, *J. Chem. Soc., Dalton Trans.*, 1973, 132.
- 19 V. T. Coombe, G. A. Heath, A. J. Mackenzie and L. J. Yellowlees, *Inorg. Chem.*, 1984, **23**, 3423.
- 20 E. König and S. Kremer, *Chem. Phys. Lett.*, 1970, **5**, 87.
- 21 J. R. Pilbrow, *Transition Ion Electron Paramagnetic Resonance*, Clarendon Press, Oxford, 1990, 93.
- 22 F. E. Mabbs and D. Collison, *Electron Paramagnetic Resonance of d Transition Metal Compounds*, Elsevier, Amsterdam, 1992, 359.
- 23 J. R. Morton and K. F. Preston, *J. Magn. Reson.*, 1978, **30**, 577.
- 24 Isotopic EPR Simulation Program, J. M. Rawson, University of Edinburgh, 1994.
- 25 N. C. Brown, G. A. Carriedo, N. G. Connelly, F. J. G. Alonso, I. C. Quarmby, A. L. Rieger, P. H. Rieger, V. Riera and M. Vivanco, *J. Chem. Soc., Dalton Trans.*, 1994, 3745.
- 26 Anisotropic EPR Simulation Program for $S = \frac{1}{2}$, F. E. Mabbs and D. Collison, University of Manchester and described in F. E. Mabbs and D. Collison, *Electron Paramagnetic Resonance of d Transition Metal Compounds*, Elsevier, Amsterdam, 1992, ch. 7.
- 27 F. E. Mabbs and D. Collison, *Electron Paramagnetic Resonance of d Transition Metal Compounds*, Elsevier, Amsterdam 1992, pp. 364–371.
- 28 A. H. Maki, N. Edelstein, A. Davidson and R. H. Holm, *J. Am. Chem. Soc.*, 1964, **86**, 6219.
- 29 N. G. Connelly, W. E. Geiger, G. A. Lane, S. J. Raven and P. H. Rieger, *J. Am. Chem. Soc.*, 1986, **108**, 6219.
- 30 B. A. Goodman and J. B. Raynor, *Adv. Inorg. Chem. Radiochem.*, 1970, **13**, 136.

Received 28th July 1995; Paper 5/05041C